Resonant magnetotunneling spectroscopy of *p*-type-well interband tunneling diodes

R. R. Marquardt, D. A. Collins, Y. X. Liu, D. Z.-Y. Ting, and T. C. McGill
Thomas J. Watson, Sr., Laboratory of Applied Physics, California Institute of Technology, Pasadena, California 91125
(Received 28 August 1995)

We report experimental results of quantum transport through InAs/AlSb/GaSb/AlSb/InAs heterostructures having well widths of 7.0, 8.0, and 11.9 nm, respectively, in magnetic fields of up to 8.0 T aligned parallel to the epitaxial growth planes. Application of this resonant magnetotunneling spectroscopy technique allows the well subband dispersions to be probed along the wave vector perpendicular to both the growth direction and the applied magnetic field. In all three samples we observe little change in the current-voltage characteristics below a sample-dependent critical magnetic field B_{crit}. Above this critical field, both the main *I-V* peak and a subsequent shoulder that forms at high fields shift in bias in a manner we attribute to be related to the HH2 and LH1 subbands (where HH and LH denote heavy and light holes), respectively. [S0163-1829(96)08719-X]

I. INTRODUCTION

Magnetic fields have proven to be a useful, if not indispensable, tool in the investigation of low-dimensional systems. In particular, the understanding of the physics of resonant tunneling in semiconductor heterostructure devices has been advanced by studies of quantum transport in the presence of magnetic fields. While magnetic fields do no work on individual charge carriers, their effect on the energy and momenta spectra allow subband structure, occupation, and dispersion to be observed experimentally.[1] With the B field aligned perpendicular to the growth plane of a semiconductor heterostructure device (parallel to the tunnel current density), the energy spectrum of the quasibound states is modified by the addition of discrete ladders of Landau levels. Studies of devices in this configuration,[2–6] and in tilted fields, with magnetic field components both parallel and perpendicular to the epitaxial layers,[7,8] investigate transport properties in systems with increased quantization and reduced dimensionality. In contrast, with a magnetic field aligned parallel to the growth plane quantization effects due to the field and the crystal potential are coaxial. Except for the highest fields, or widest quantum wells, the magnetic field in this geometry may be treated perturbatively. As a result, the device operates without additional quantization or significant modification to the eigenstates and energies of the system; the only effect of the field, semiclassically, is to bend the carrier trajectories into cyclotron orbits about the axis of the field. This alteration of the carrier distribution in momentum space is exploited in resonant magnetotunneling spectroscopy[9] (RMTS) to probe the energy subband dispersion in semiconductor quantum wells.

While a majority of work with the RMTS technique has been in the study of traditional intraband tunneling diodes,[9–13] relatively few observations have been reported for interband devices employing the InAs/GaSb type II broken-gap band alignment. Although the unique properties of InAs/GaSb heterostructures have been known for some time,[14] only recently have these been exploited in the creation of a new class of quantum transport device.[15,16] Figure 1 shows the band alignments of an InAs/AlSb/GaSb/AlSb/InAs double barrier structure [*p*-type-well resonant interband tunneling (RIT) diode] at room temperature. Because of the type II nature of the band offset between InAs and GaSb, the conduction-band edge of InAs lies 0.15 eV lower in energy than the valence-band edge of GaSb.[17] Transport through this system involves resonant tunneling of electrons from the InAs emitter, through unoccupied electron states in the subbands of the GaSb well, and subsequently back into the conduction band of the collector. Observations of magnetotunneling in interband devices have focused primarily on the converse of the device in Fig. 1, with an InAs well and GaSb electrodes (*n*-type-well RIT),[18–20] or have investigated the barrierless InAs/GaSb/InAs system with the magnetic field perpendicular to the layers.[21] We report the results of RMTS investigations of *p*-type-well RIT devices in fields of up to 8.0 T. In Sec. II A we detail the samples studied and

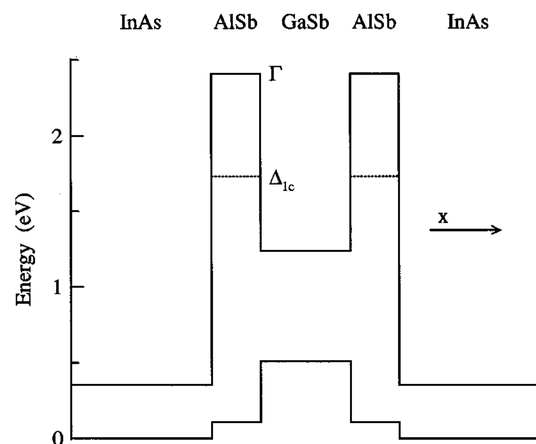

FIG. 1. Energy-band diagram of an InAs/AlSb/GaSb/AlSb/InAs resonant interband tunneling diode (*p*-type-well RIT) at 300 K. The conduction-band minimum of InAs lies 0.15 eV below the valence-band maximum of GaSb prior to band bending induced by the transfer of charge between the broken-gap layers. AlSb is an indirect gap semiconductor; both the Γ and near-*X* minima are shown. Quantum transport across the device occurs via resonant tunneling of emitter electrons through unoccupied electron states in the GaSb well.

 © 1996 The American Physical Society

TABLE I. Growth parameters for the three samples investigated.

Material	Thickness	Doping
n^+-InAs	>0.25 μm	3×10^{18} cm^{-3}
n-InAs	50.0 nm	1×10^{17} cm^{-3}
InAs	5.0 nm	undoped
AlSb	4.0 nm	undoped
GaSb	7.0, 8.0, 11.9 nm	undoped
AlSb	4.0 nm	undoped
InAs	5.0 nm	undoped
n-InAs	50.0 nm	1×10^{17} cm^{-3}
n^+-InAs	>1.2 μm	3×10^{18} cm^{-3}

the experimental setup and technique. Our measurements are presented in Sec. II B, and analyzed in Sec. III. We summarize and conclude in Sec. IV.

II. EXPERIMENT

A. Experimental setup

Three p-type-well RIT samples, grown by molecular beam epitaxy[22] on (100) n^+-GaAs substrates, were investigated. The three devices, having well widths of 7.0 nm (device A), 8.0 nm (device B), and 11.9 nm (device C), were otherwise grown with identical layer thicknesses and doping. These device parameters are summarized in Table I. Devices A and B each had octagonal mesa cross sections, 150 μm across, with a total area of 17 300 μm^2. Device C was fabricated with a 100-μm-square mesa geometry. Devices A, B, and C had zero-field peak current densities of 126, 44, and 138 A/cm^2, respectively, at 4.5 K. The higher current densities in samples A and C may be indicative of greater nonresonant leakage current in these devices. The peak-to-valley ratios (PVR's) of all three were low, typically 2–8:1, at 4.5 K. These PVR's are low even for devices of this size, and are indicative of enhanced inelastic transport across the quantum-well region.

The data were acquired with a Hewlett-Packard 4145A semiconductor parameter analyzer at a constant sample temperature of 4.5 K using standard current-voltage (I-V) measurement techniques. All I-V curves were scanned from low to high voltage, although typically no more than 2–3 mV of hysteresis was observed when the scan direction was reversed. Most of the mesas displayed nearly symmetric I-V curves, but in all cases the mesa and polarity with the highest PVR at 4.5 K was selected for study. The header-to-4145A series resistance was measured to be 1.4 Ω at 4.5 K, and the total resistance in series with the devices was estimated not to exceed 2.5 Ω from point-to-point measurements on the lower InAs electrode layer. For each device, I-V curves from 0.0 to 0.5 V were taken in 1-mV steps at regularly spaced (0.1 T) magnetic fields from 0.0 to 8.0 T.

B. Measurements

A typical zero-field current-voltage characteristic from device B at 4.5 K is shown in Fig. 2(a). The I-V curve of the same device in an 8-T field is shown in Fig. 2(b). Many of the general trends seen in all three samples are evident in

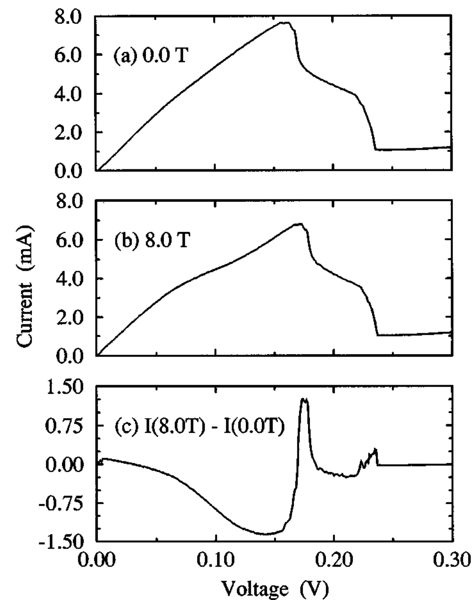

FIG. 2. Example current-voltage curves for device B at (a) 0.0 T and (b) 8.0 T. The magnetic field shifts the peak to higher voltage, while pushing out a shoulder to lower bias. In addition, the peak current has decreased. The position and magnitude of the valley current are unchanged by the magnetic field. The difference spectrum, shown in (c), is formed by the subtraction of the 0.0-T data from the 8.0-T data. The resulting spectrum indicates the net effect of the applied magnetic field on the conduction of the device at any given bias. In turn, this change in conduction reflects the shift in distribution of charge carriers along the parallel dispersion of the well, as argued in Sec. III.

these data. First, at high fields, a shoulder forms and moves rapidly to lower voltages with increased applied magnetic field. In addition, the peak of the I-V curve shifts, less dramatically, to higher bias. The peak current was observed to decrease with increasing applied field in samples A and B, while in sample C the peak current was constant until it was observed to increase in magnetic fields above 6 T. The peak current was never observed to change by more than $\approx 10\%$ of its zero-field value.

Figure 3 shows the peak and shoulder positions for each sample plotted as a function of applied field. The shoulder position was determined from a local minimum of the conductance curves for each sample. In cases where a broad peak appeared to contain multiple maxima, each position is shown. These are plotted to indicate the voltage range over which the main peak was ambiguously located, and are not interpreted as attributable to distinct quantum mechanical resonances. For all samples, the behavior is similar; there is little, if any, appreciable change at low fields until some critical field (B_{crit}) is exceeded, at which point both the main peak and subsidiary shoulder are observed to shift in voltage with changing applied magnetic field. The shift of the main peak saturates at high fields and is not seen to change in any of the samples at fields greater than 7 T. The shoulder position, however, appears to be a linear function of magnetic field in all three samples. For device A, a linear regression of the shoulder position yielded a slope of -18.9 ± 0.3 mV/T, with a squared correlation coefficient r^2 of 0.996. Regressions of devices B and C found slopes of -21.3 ± 0.5 mV/T

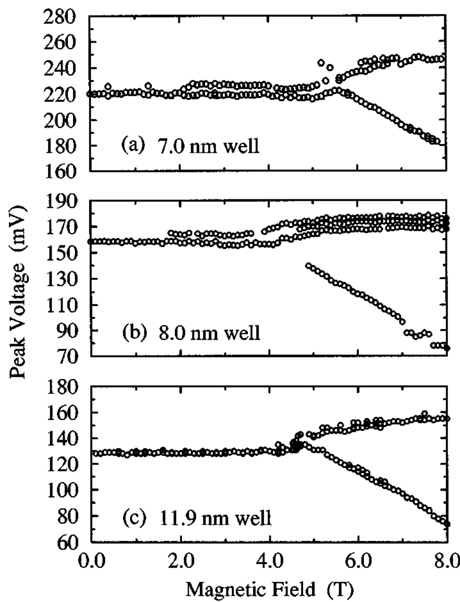

FIG. 3. Peak and shoulder voltages as a function of applied magnetic field for devices A, B, and C, respectively. Little change is observed for fields below some sample-dependent critical value. Above this critical field, the peak voltage appears to saturate at high fields, whereas the location of the shoulder is a linear function of applied field for all three devices.

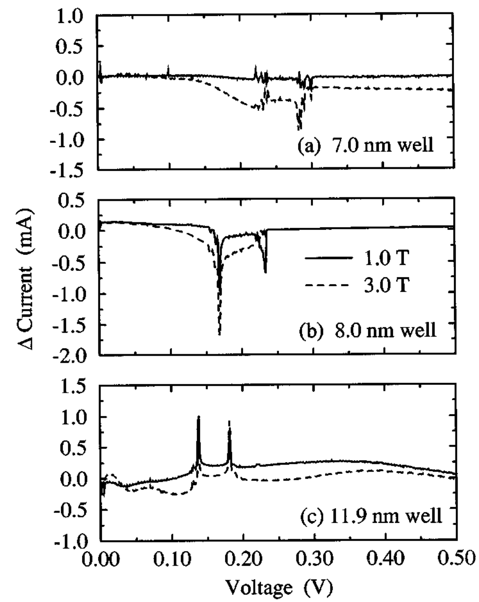

FIG. 4. Difference spectra for samples A, B, and C, respectively, at both 1.0 and 3.0 T, below the critical field of each sample. Each spectrum is obtained by subtracting the zero-field current-voltage characteristic from the same data taken at the given magnetic field. Below the critical field, there are slight changes in the observed behavior of each sample not evident in the I-V peak position.

($r^2=0.986$) and -18.8 ± 0.3 mV/T ($r^2=0.992$), respectively. The slopes for devices A and C are therefore statistically identical, whereas that of device B is more than 10% greater.

Unlike the data from typical RMTS investigations of traditional intraband tunnel devices, much of the structure of the subbands in the GaSb well is missing from the data in Figs. 2(a), 2(b), and 3. In intraband devices, multiple peaks, each associated with a separate subband, can be tracked with applied magnetic field to trace the $k_{\parallel}$ well dispersion. In interband devices, the opposite dispersions of the electrode and the well in interband devices, as well as the narrow voltage window in which negative differential resistance (NDR) can occur, result in resonant transmission through several well states at the same bias. The resulting I-V curve is a complicated convolution of the contributions of the various well states. Consequently, we found it necessary to examine the difference spectra, such as shown in Fig. 2(c), of the three devices over the range of investigated fields, so as to separate the changes in conduction induced by the applied field from the complexities of the zero-field transport. Additionally, each of these spectra details the effect of the magnetic field more completely than the simple plot of peak positions shown in Fig. 3. Figures 4 and 5 detail the difference spectra for the three samples at low and high fields, respectively. It should be noted that below the critical field, there is relatively little nonzero contribution to the difference spectra, as shown in Fig. 4. In contrast, above B_{crit} there is great variation in the difference spectra with applied field, detailed in Fig. 5. Each difference spectrum was formed by subtracting the zero-field current-voltage data for each device from the I-V curve at a given magnetic field. This spectrum may be positive or negative since the shift in carrier distribution caused by the magnetic field both adds and removes conduction channels at a given bias relative to the zero-field equilibrium distribution. The difference spectrum in Fig. 2(c) is typical of all three samples. The NDR region is demarked by two peaks in the spectrum, each indicating additional current

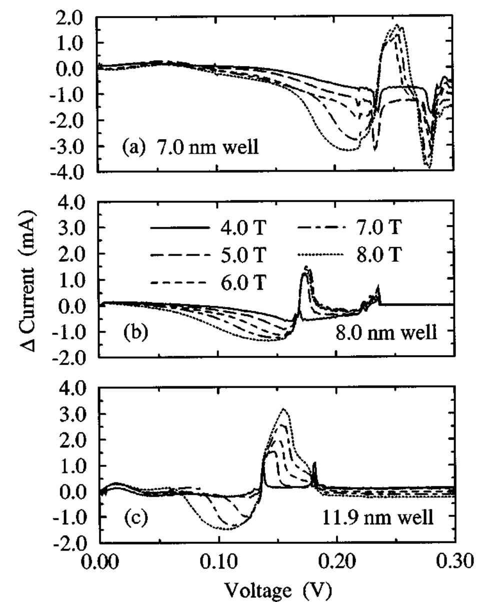

FIG. 5. Difference spectra for samples A, B, and C, respectively, at 4.0, 5.0, 6.0, 7.0, and 8.0 T, at or above the critical field of each sample. Each spectrum is obtained by subtracting the zero-field current-voltage characteristic from the same data taken at the given magnetic field. In this regime, at or above the critical magnetic field, each sample displays distinct behavior. The transport characteristics of all three samples, however, show a far greater dependence on magnetic fields greater than B_{crit}.

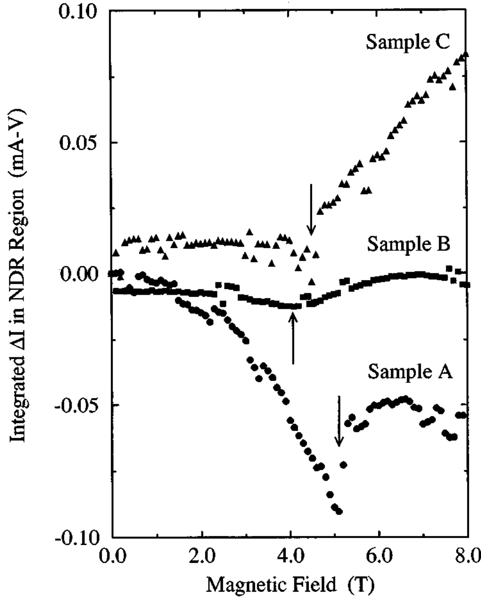

FIG. 6. The change in device current integrated over the NDR region (as defined for each sample) plotted as a function of magnetic field. The apparent critical magnetic fields are indicated by arrows. The critical fields so obtained agree well with values derived from Fig. 3. The abrupt nature of this transition is evident in samples A and C.

at those biases. When the peak or valley voltage shifts, as in this case with an 8.0-T field, the subtraction necessary to form the difference spectrum mimics the calculation of the finite element approximation to the local derivative, and thus in regions of large $|dI/dV|$ the difference spectrum has narrow peaks (or valleys, depending upon the sign of the peak shift). An examination of the difference spectra of the three samples highlights their differing subband structure and the effect of the magnetic field on resonant transport.

While the critical field B_{crit} for each sample can be estimated from Fig. 3, it is more easily obtained by looking at the integrated area of the difference spectra in the NDR region of the sample, as a function of applied field. These data are shown in Fig. 6; the three critical fields are marked by arrows. Devices A and C show very sharp discontinuities in the region of their critical fields, between 5.1–5.2 T and 4.5–4.6 T, respectively. These values are in good agreement with the data in Fig. 3. The data for device B show no discontinuity, but rather a smooth transition, at a critical field of approximately 4.1–4.2 T. The critical field does not, therefore, seem to depend monotonically on well width. Samples A and C also displayed additional behavior at their respective critical fields not evident in sample B. For these samples, a significant second peak, located in the NDR region, was observed to appear abruptly as the field was increased above B_{crit}. We are unable to rule out circuit oscillations or hysteresis known to exist in the NDR region of resonant tunneling diodes[23,24] as the cause of this phenomenon. However, the exact field at which this extra peak is observed has been reproducibly determined to the resolution limit of the magnet, roughly 50 G at these fields. Furthermore, this phenomenon appears to occur at the critical field B_{crit}, at which the gross RMTS behavior of the samples likewise abruptly changes. Both samples in which this second peak was observed (A and C) have a sharp cusp in the NDR integral at the critical field, whereas sample B displays neither of these behaviors.

III. ANALYSIS

The theory of resonant magnetotunneling spectroscopy[9,25,26] is similar for tunneling mechanisms involving initial and final states with either the same, or opposite, energy dispersions. Thus, the theory for both may be developed in tandem. Referring to Fig. 1, we take the x axis to lie along the growth direction, while the y and z axes both lie in the plane parallel to the heterointerfaces. With the B field along the z axis, $\vec{B}=B\hat{z}$, and using the Landau gauge vector potential $\vec{A}=Bx\hat{y}$, the sole effect of the field on the Hamiltonian is to replace the canonical crystal momentum operator $\mathbf{p}$ with $\mathbf{p}-q\mathbf{A}$. Assuming the vector potential term can be treated as a perturbation, the eigenstates of the Hamiltonian remain unchanged to first order, and the mechanical momentum along the y axis is increased by $eB\langle x\rangle/\hbar$, where $\langle x\rangle$ is the expected value of the position operator averaged over a given localized state under the perturbation. The origin along the x axis is arbitrary; a change in origin amounts to a change of gauge, for which the physics is invariant. Changes in $\langle x\rangle$, however, such as tunneling from a localized emitter notch state to a quasibound state in the well, result in an increased mechanical momentum along the y direction. The conjugate momentum, $p_y \equiv \hbar k_y$, however, remains conserved in elastic transport. The parallel energy dispersions of the well states, dependent upon the mechanical momentum, $M_y = p_y + eB\langle\Delta x\rangle$, are shifted in k space when plotted against the conserved quantity k_y as shown in Fig. 7. As the magnetic field is increased, and the mechanical momentum is likewise boosted, the well states are further shifted along k_y, changing the quasibound states available for elastic tunneling processes conserving both E and k_y. An ensemble of electrons, thermalized in an emitter subband such that $|k_y| \leq k_F$ and $M_y = p_y = \hbar k_y$, will have mechanical momenta distributed from $-k_F + eB\langle\Delta x\rangle/\hbar$ to $k_F + eB\langle\Delta x\rangle/\hbar$ after tunneling an expected distance $\langle\Delta x\rangle$ to a localized quasibound state in the well. The magnetic field, doing no work on the charge carriers, cannot alter their energies. The applied voltage required to meet the resonance condition for elastic tunneling is altered in the presence of the magnetic field. As the well states are shifted, the energy dispersion of the destination states in the well changes the energy required for resonance at a given k_y. Thus, as a function of applied magnetic field, the current-voltage (I-V) characteristics of the device should be affected in a manner that is fundamentally related to the energy dispersion of the subbands in the well.

For devices in which the initial and final states are of similar dispersion, peaks in the I-V curves can be associated with the energy of a given subband dispersion at a $k_{\parallel}$ value equal to the increase in mechanical momentum induced by the applied magnetic field, $\Delta M_y = eB\langle\Delta x\rangle$.[9] Graphically, this criterion is shown for intraband tunneling devices in Fig. 7. In the absence of any magnetic field, the peak in the I-V characteristic corresponds to the condition that the $k_{\parallel}$ band edges of the well and electrode dispersions are coincident in

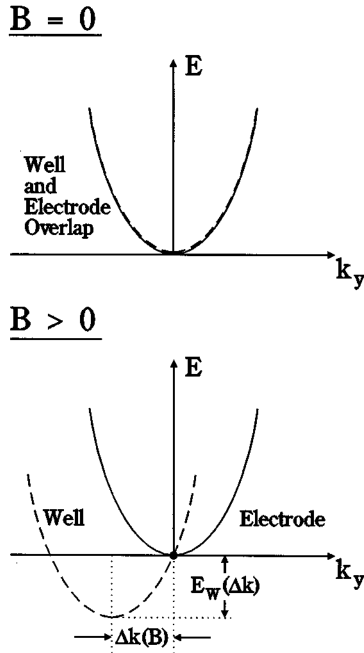

FIG. 7. Electrode and well dispersions in the k_y direction (for $k_x = 0$) in the effective-mass approximation for an intraband double barrier structure, with and without a magnetic field applied perpendicular to the tunnel current. Both cases are shown at the peak current bias, with states meeting the elastic tunneling condition at the highlighted overlap. The well subband dispersion is shifted by a $\Delta k(B)$ linearly proportional to the magnetic field, increasing the peak voltage by $E_W(\Delta k)$. While the effective mass approximation is suitable to describe intraband tunneling and the RMTS experiment in n-type structures, it should be noted, for limited regions of k space, that p-type intraband tunneling can involve bands of opposite dispersion in much the same manner as interband tunnel structures.

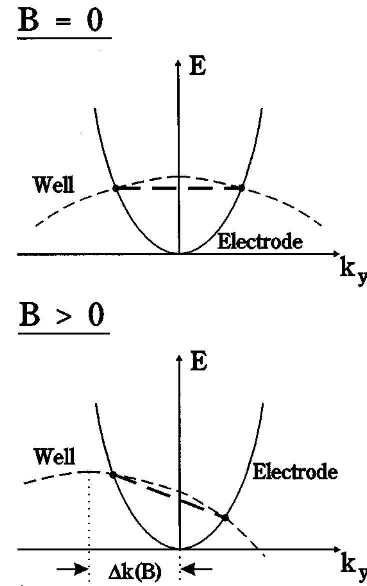

FIG. 8. Electrode and well dispersions in the k_y direction (for $k_x = 0$) in the effective-mass approximation for the investigated p-type-well interband RIT structure, with and without a magnetic field applied perpendicular to the tunnel current. The overlap at any given bias involves a distribution of values in k_y, as indicated by the thick dashed lines. Experimental RMTS data for this device therefore cannot be attributable to a single, field-dependent parallel wave vector.

energy, as shown. In a magnetic field, the well state is shifted along the k_y axis, and, as the figure shows, the I-V peak again occurs at $k_y = 0$ (with $|k_x| \leq k_F$), where the electrode has the greatest number of carriers available for tunneling. The degree to which the peak voltage is shifted is therefore given by the well dispersion in the k_y direction at a relative wave vector $eB\langle \Delta x \rangle/\hbar$ from the well state band edge. Thus, plotting the change in peak voltage (or, equivalently, simply the peak voltage itself) as a function of the applied magnetic field traces out the parallel band structure of the quasibound state in the well. From this argument, it is clear that the well dispersion need not obey the parabolic band approximation, and the technique is capable of mapping complicated well band structures.

The mechanics of interband tunneling are, unfortunately, far more complex, and they obscure the direct interpretation of the experimental results. The opposite dispersions of the electrode and well result in elastic tunneling through a broad distribution of states in k space at a single bias. As shown in Fig. 8, in the absence of a magnetic field the two dispersions have coincident energies and momenta at two values along the k_y axis (for $k_x = 0$), symmetrically located about $k_y = 0$. With the consideration of nonzero k_x as well, the overlap between the two bands involves all k_y values between these extrema. It can be shown in the parabolic band approximation that, in general, the set of elastically allowed states is a circle in the $k_\parallel$ plane, centered along the k_x axis at $k_x = 0$, and along the k_y axis at

$$K_0 = \frac{m_E^\star \delta}{m_W^\star + m_E^\star}, \tag{1}$$

having a radius,

$$K_R = \sqrt{\frac{\Delta E_0 - [eV + \hbar^2 \delta^2 / 2(m_W^\star + m_E^\star)]}{\hbar^2 / 2\mu^\star}}, \tag{2}$$

where ΔE_0 is the zero-field difference in the $k_\parallel = 0$ band edges, $m_E^\star$ and $m_W^\star$ are the electrode and well effective masses, respectively, δ is the field-induced increase in the mechanical momentum along the k_y direction $(= eB\langle \Delta x \rangle/\hbar)$, V is the applied bias, and $\mu^\star$ is the reduced mass of the electrode and well dispersions. As shown in the figure, this intersection occurs over a range of energies as well. As the magnetic field is increased, k space is sampled in a region centered about a k_y value that is dependent upon the masses of both dispersions and linearly proportional to the applied field. Thus, while this shift in k_y results in changes to many of the factors determining the tunnel current, including the number of states involved, and their quantum mechanical transmission probabilities, we expect the change in peak voltage to be related, albeit in a complex manner, to the well (and electrode) dispersions. While the difference spectrum contains more information than does the position of the I-V peak, we do not have a theory of adequate sophistication to model the effect of the magnetic field on the entirety of the current-voltage characteristic. Therefore, we

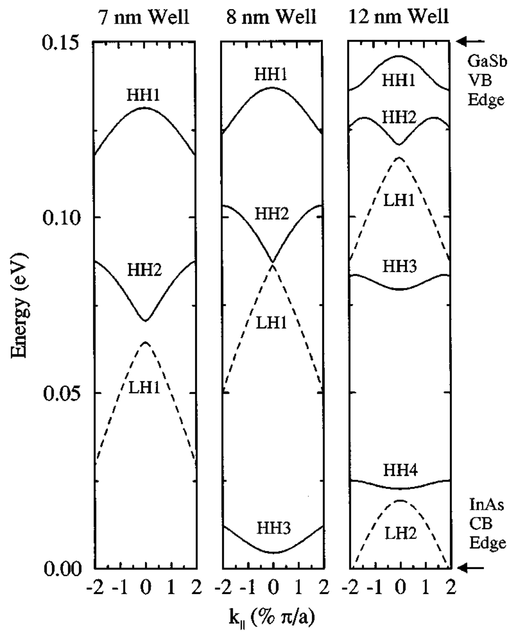

FIG. 9. Theoretical zero-field well subband structure for RIT devices having GaSb well widths of 7.0, 8.0, and 12.0 nm, respectively, in the energy range between the InAs conduction-band edge and GaSb valence-band edge. The parameter a is the cubic lattice constant for GaSb, equal to 0.6095 nm. Based upon the calculated quantum mechanical transmission coefficients (not shown), the majority of the resonant current tunnels through the HH2 and LH1 subbands.

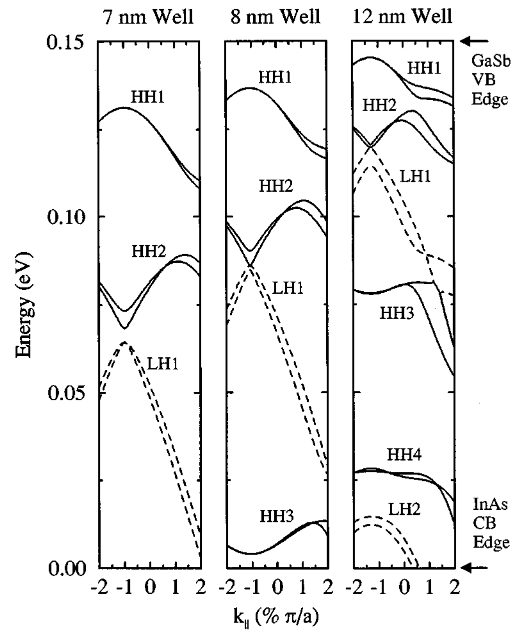

FIG. 10. Theoretical well subband structure for RIT devices having GaSb well widths of 7.0, 8.0, and 12.0 nm, respectively, at a magnetic field of 8.0 T. The parameter a is the cubic lattice constant for GaSb, equal to 0.6095 nm. The maximum $k_{\|}$ values that may be probed at 8.0 T (in units of $\% \pi/a$) are 0.99%, 1.02%, and 1.13%, for samples A, B, and C, respectively. The predicted shift of the well subbands is shown, along with the additional features induced by the applied field.

are limited to a semiqualitative analysis of the peak shifts relative to the theoretical band structure.

Figures 9 and 10 show the theoretical parallel band structure of the three samples investigated experimentally, at 0.0 and 8.0 T, respectively. These dispersions were calculated using an efficient, numerically stable 8-band $\mathbf{k}\cdot\mathbf{p}$ method generalized to include magnetic fields.[27] Figure 9 demonstrates the complexity of the well subbands in this device structure, even in the absence of magnetic fields. At each bias, emitter carriers couple to more than one hole subband. Hence, the distinct I-V peaks expected are broadened into a single peak. As can be seen in Fig. 10, the addition of the magnetic field complicates the situation even further. Clearly, the field has more effect than to simply shift the bands in k space. There is a great deal of interaction between the subbands, in addition to lifting of the spin degeneracy. From the basis of the well width dependent shift of the band edges, theory predicts that $\langle \Delta x \rangle$ is ≈ 11 nm$+b+w/2$, where b and w are the barrier and well widths, respectively. In addition to the complexities of the subband structure, the quantum mechanical couplings between the electrode states vary quite strongly between bands and, to a lesser degree, as a function of $k_{\|}$. Consequently, the HH2 (where HH denotes heavy hole) band provides a greater transmission channel than either the HH1 or HH3 bands. Additionally, the LH (light hole) bands have wider (in energy) transmission peaks at any given $k_{\|}$, and thereby offer the greatest integrated coupling to the electrode, and the most likely path for elastic tunneling. As a result, it is suggestive that the movements of the peak and shoulder in the experimental I-V data for fields greater than B_{crit} correspond in some manner to the HH2 (for the peak) and LH1 (for the shoulder) subbands, subject to the previously mentioned caveats. The movement of the shoulder was in fact consistent with a lighter mass negative dispersion, and that of the peak similarly consistent with a heavier, positive dispersion, as found in Figs. 9 and 10 for the LH1 and HH2 subbands, respectively. The theory indicates that for the widest well, the LH1 and HH3 bands interact strongly, but it is doubtful that the experimental results should be capable of distinguishing this behavior from the general, low mass trend of the coupled bands.

The behavior of the experimental results at fields equal to and below the critical field is incongruent with the semiclassical analysis presented. The magnetic field has little outward effect on the experimental results at values less than B_{crit}. Additionally, the transition at the critical field is hyperabrupt, experimentally distinguishable down to the resolution limit of the magnet, roughly 50 G. The sharp distinction between behavior above and below the critical field raises a number of questions. This phenomenon has not been reported in earlier RMTS investigations of intraband devices, and was not seen with our apparatus in the investigation of transport in an InAs/AlSb double barrier heterostructure. It would therefore seem that this behavior is attributable to the interband nature of transport in the InAs/GaSb/AlSb system. We have yet to determine an explanation for this observed failure of the semiclassical RMTS model over a large range of magnetic fields.

IV. CONCLUSIONS

We have presented results of resonant magnetotunneling spectroscopy experiments on p-type-well, interband InAs/

AlSb/GaSb/AlSb/InAs tunnel structures. Three samples were investigated, having identical growth parameters save for well widths of 7.0, 8.0, and 11.9 nm, respectively. Current-voltage characteristics of these structures were examined in magnetic fields of up to 8.0 T applied perpendicular to the growth direction. Below a critical magnetic field, B_{crit}, little fundamental change was seen in any of the samples. However, at and above this critical field, the single peak in the I-V characteristic of each sample was found to shift to higher bias, and, in addition, a shoulder was observed to form and move to low bias in increasing magnetic fields. The critical field appears to represent a boundary between a low-field regime for which the increased magnetic field has essentially no effect on the I-V characteristic, and a high-field regime in which both the main peak and the shoulder move in a manner consistent with the semiclassical RMTS theory. The critical field was not observed in the study of transport of an InAs/AlSb double barrier device with the same apparatus, suggesting that the critical field is unique to the interband tunnel devices. The change in behavior of two of the devices (those with 7.0- and 11.9-nm wells) at the critical field was abrupt and resulted in a very distinct difference in observed transport characteristics, whereas those of the third were more gradually altered at B_{crit}. This distinction between the samples is most likely attributable to differences in growth or processing conditions affecting elastic transport in the 8.0-nm well sample, and not to differences in well width. In addition to these raw measurements of the peak and shoulder voltages, difference spectra were shown to detail further the effect of the applied field on transport.

The complex nature of the interband tunneling mechanism was shown to lead to a complicated, and indirect, relationship between the observed effects of the magnetic field and the parallel subband dispersions of the quasibound states in the well. As interband transport at a given bias involves a broad spectrum of states in both the k_x and k_y directions, and the resultant effect of the field upon the peak position involves changes in the number of states tunneling, their respective energies, and their quantum mechanical transmission probabilities, the observed peak shift cannot be uniquely assigned to the well dispersion at a field-dependent wave vector, as it can for typical intraband transport. However, as argued in Sec. III, we believe that in comparison with multiband theoretical calculations, it is most likely that the peak and shoulder positions above B_{crit} correspond to the HH2 and LH1 subbands, respectively.

The data presented raise interesting questions as to the nature of transport in interband tunneling devices. The abrupt, catastrophic changes observed at the critical field are not understandable within the semiclassical theory invoked to explain RMTS experiments. We are pursuing alternate explanations to better understand both this phenomenon and quantum transport in this system in general. Further observations are warranted at higher magnetic fields, both to study the peak shifts further, and to also lend further insight into the nature of the observed critical magnetic field.

ACKNOWLEDGMENTS

The authors would like to thank J. F. Swenberg and M. W. Wang for helpful discussions and assistance. One of us (R.R.M.) would like to acknowledge the partial financial support of the National Science Foundation. This work is supported by the Office of Naval Research under Grant No. N00014-89-J-1141.

[1] For reviews of the basic effects of magnetic fields in two-dimensional semiconductor systems, see L. L. Chang, in *Molecular Beam Epitaxy and Heterostructures*, Vol. 87 of *NATO Advanced Study Institute, Series E: Applied Sciences*, edited by L. L. Chang and K. Ploog (Martinus Nijhoff, Dordrecht, 1985); G. Bastard, *Wave Mechanics Applied to Semiconductor Heterostructures* (Les Éditions de Physique, Les Ulis, France, 1988).

[2] E. E. Mendez, L. Esaki, and W. I. Wang, Phys. Rev. B **33**, 2893 (1986).

[3] V. J. Goldman, D. C. Tsui, and J. E. Cunningham, Phys. Rev. B **35**, 9387 (1987).

[4] L. Eaves *et al.*, Appl. Phys. Lett. **52**, 212 (1988).

[5] C. E. T. Gonçalves de Silva and E. E. Mendez, Phys. Rev. B **38**, 3994 (1988).

[6] E. E. Mendez, H. Ohno, L. Esaki, and W. I. Wang, Phys. Rev. B **43**, 5196 (1992).

[7] J. J. Koning *et al.*, Phys. Rev. B **42**, 2951 (1990).

[8] M. L. Leadbeater, F. W. Sheard, and L. Eaves, Semicond. Sci. Technol. **6**, 1021 (1991).

[9] R. K. Hayden *et al.*, Phys. Rev. Lett. **66**, 1749 (1991).

[10] J. P. Eisenstein, T. J. Gramila, L. N. Pfeiffer, and K. W. West, Phys. Rev. B **44**, 6511 (1991).

[11] S. Y. Lin *et al.*, Appl. Phys. Lett. **60**, 601 (1992).

[12] U. Gennser *et al.*, Phys. Rev. Lett. **67**, 3828 (1991).

[13] T. Osada, N. Miura, and L. Eaves, Solid State Commun. **81**, 1019 (1992).

[14] L. L. Chang and L. Esaki, Surf. Sci. **98**, 70 (1980).

[15] D. H. Chow *et al.*, in *Quantum-Well and Superlattice Physics III*, SPIE Proceedings No. 1283 (SPIE, Bellingham, WA, 1990).

[16] D. A. Collins *et al.*, in *Resonant Tunneling in Semiconductors: Physics and Applications*, edited by L. L. Chang, E. E. Mendez, and C. Tejedor (Plenum, New York, 1991).

[17] G. J. Gualtieri, G. P. Schwartz, R. G. Nuzzo, and W. A. Sunder, Appl. Phys. Lett. **49**, 1037 (1986); G. J. Gualtieri *et al.*, J. Appl. Phys. **61**, 5337 (1987).

[18] E. E. Mendez, in *Resonant Tunneling in Semiconductors: Physics and Applications* (Ref. 16).

[19] E. E. Mendez, J. Nocera, and W. I. Wang, Phys. Rev. B **45**, 3910 (1992).

[20] E. E. Mendez, Surf. Sci. **267**, 370 (1992).

[21] T. Takamasu *et al.*, Surf. Sci. **263**, 217 (1992).

[22] D. A. Collins *et al.*, Appl. Phys. Lett. **57**, 683 (1990).

[23] V. J. Goldman, D. C. Tsui, and J. E. Cunningham, Phys. Rev. Lett. **58**, 1256 (1987).

[24] T. C. L. G. Sollner, Phys. Rev. Lett. **59**, 1622 (1987).

[25] R. Winkler and U. Rossler, Surf. Sci. **305**, 295 (1994).

[26] G. Goldoni and A. Fasolino, Solid State Electron. **37**, 991 (1994).

[27] Y. X. Liu, D. Z.-Y. Ting, and T. C. McGill (unpublished).